LIST OF FIGURES

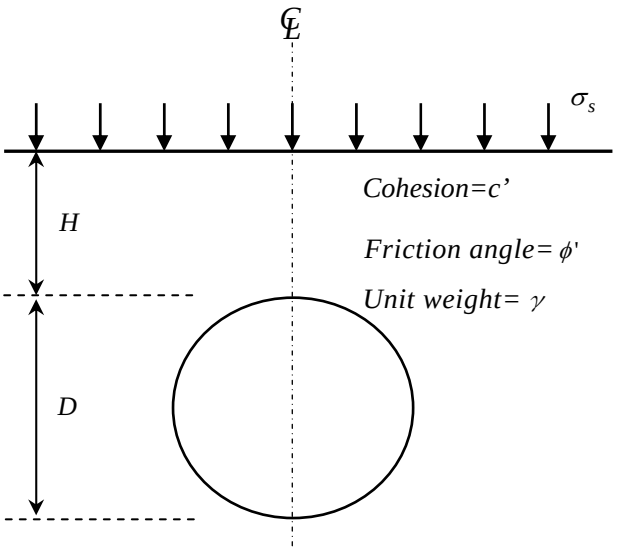

Fig. 1. Plane strain circular tunnel in cohesive-frictional soil.

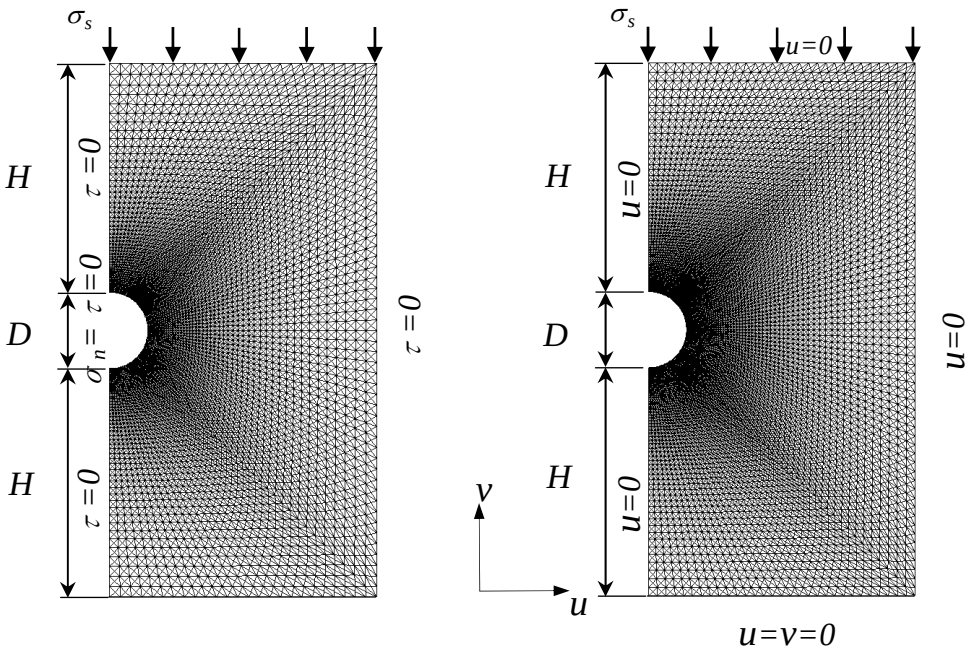

(a) Lower-bound mesh (b) Upper-bound mesh

Fig. 2. Typical finite element meshes for a circular tunnel (*H/D*=3, rough interface).

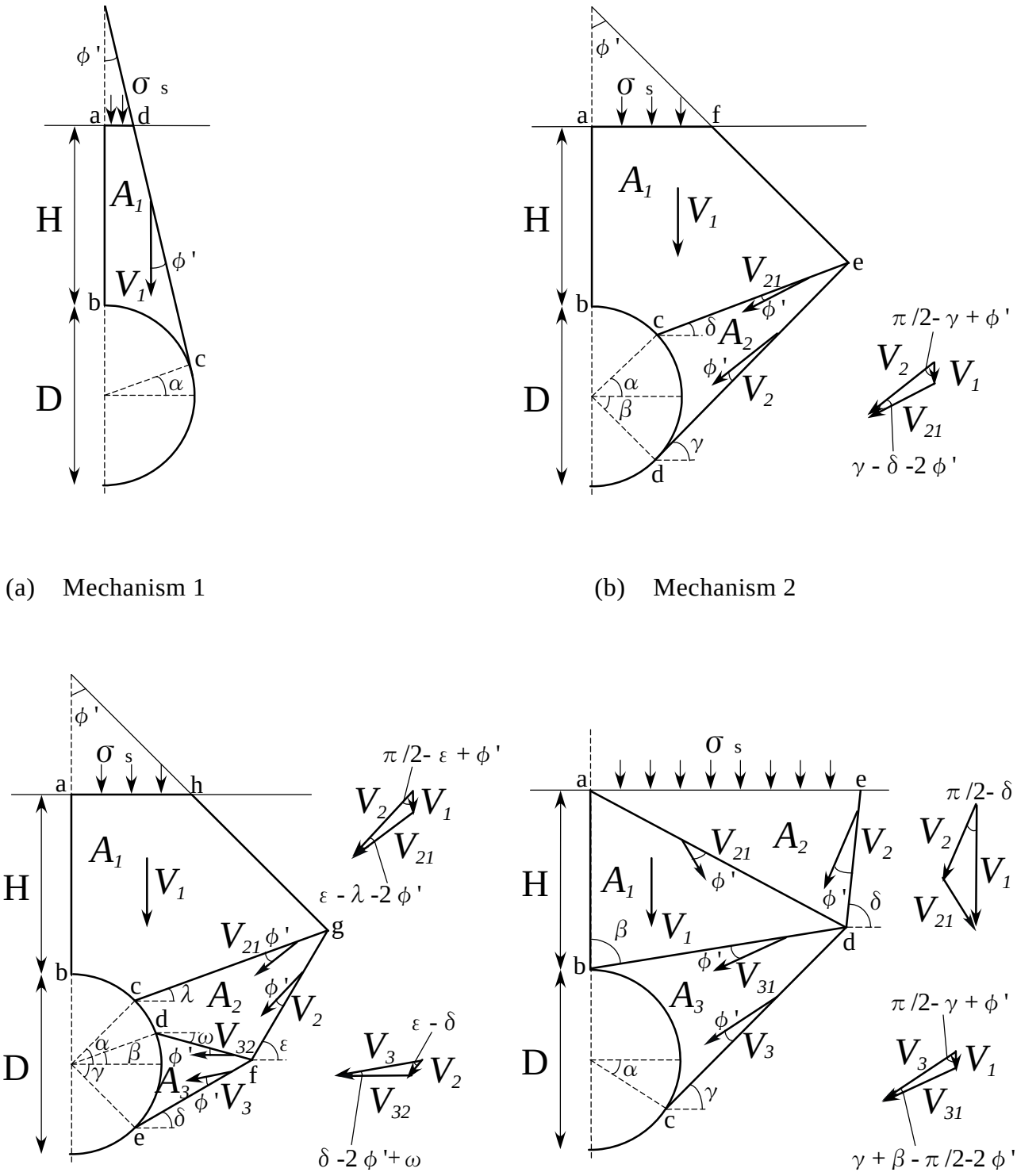

Fig. 3. Upper-bound rigid-block mechanisms for a circular tunnel.

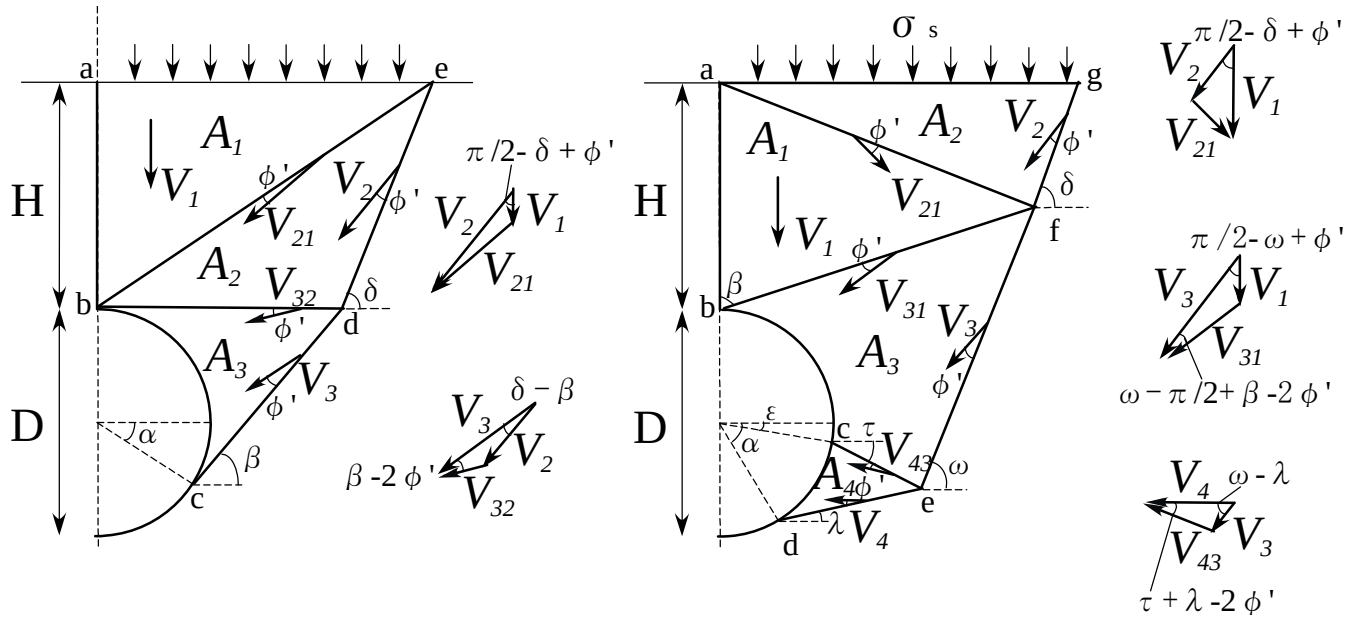

(e) Mechanism 5 (f) Mechanism 6

Fig. 3. Upper-bound rigid-block mechanisms for a circular tunnel.

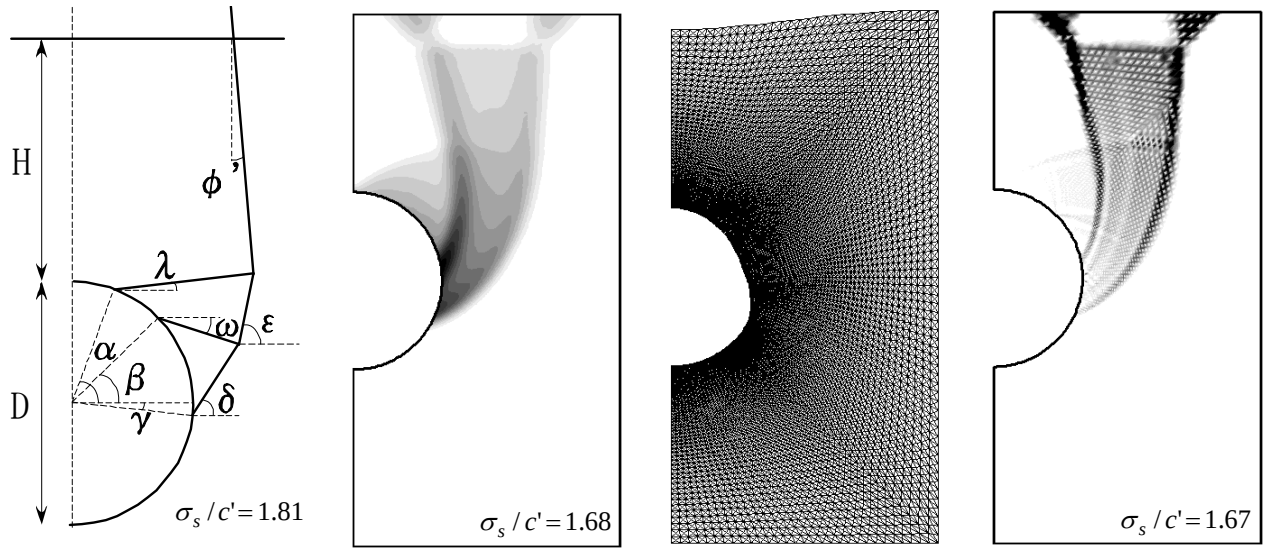

(a) Rigid-block mechanism (b) Power dissipation (c) Deformed mesh (d) Plastic multiplier field

Fig. 4. Comparison of rigid-block mechanism with finite element limit analysis (H/D=1, ϕ'=5°, $\gamma D/c'$=1, smooth interface).

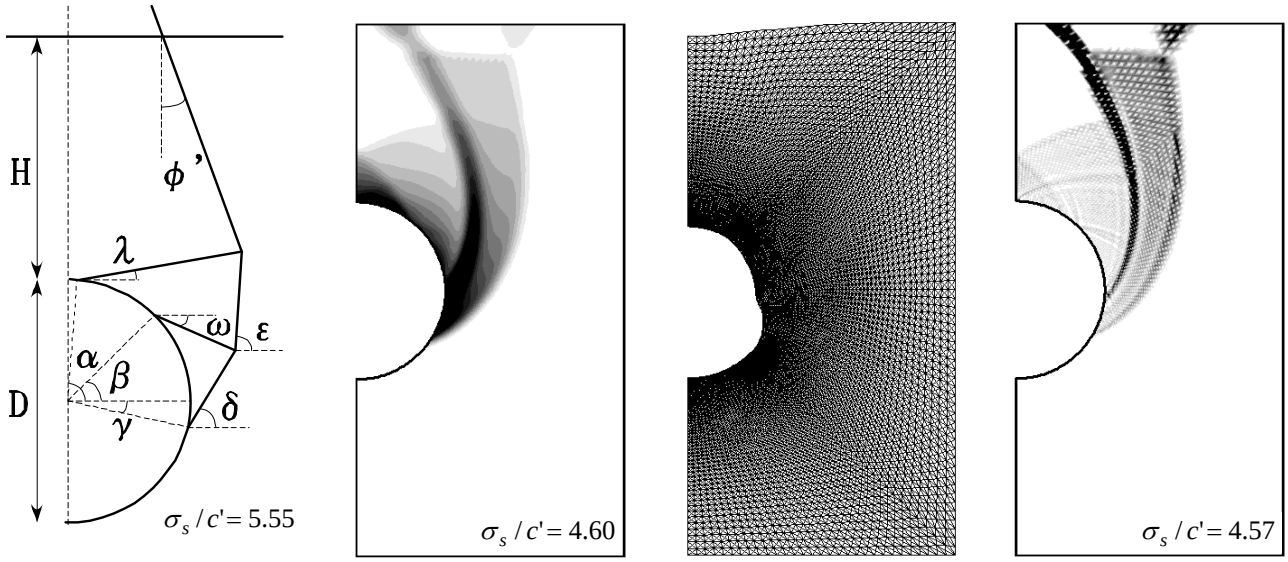

(a) Rigid-block mechanism (b) Power dissipation (c) Deformed mesh (d) Plastic multiplier field

Fig. 5. Comparison of rigid-block mechanism with finite element limit analysis (H/D=1, ϕ'=20°, $\gamma D c'$=1, smooth interface).

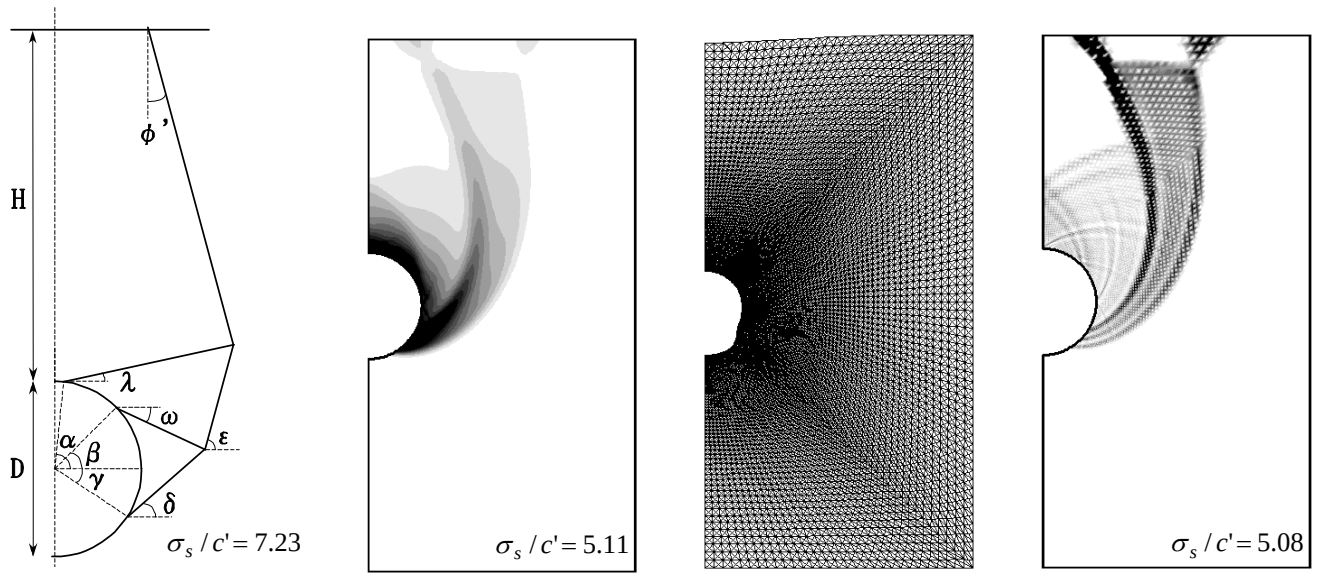

(a) Rigid-block mechanism (b) Power dissipation (c) Deformed mesh (d) Plastic multiplier field

Fig. 6. Comparison of rigid-block mechanism with finite element limit analysis (H/D=2, ϕ'=15°, $\gamma D/c'$=1, smooth interface).

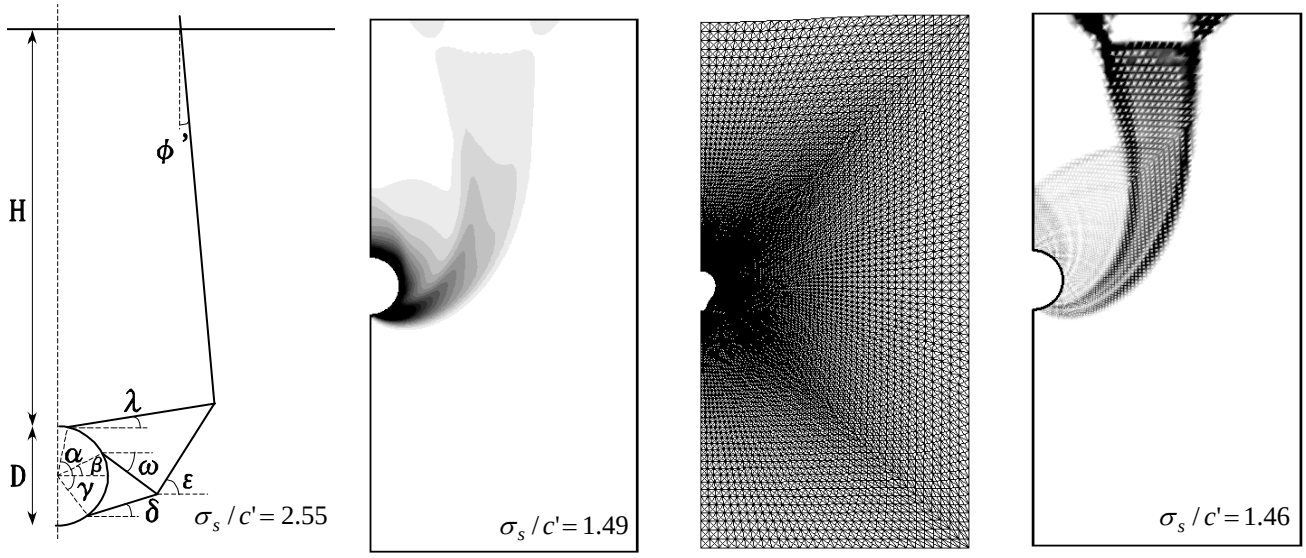

(a) Rigid-block mechanism (b) Power dissipation (c) Deformed mesh (d) Plastic multiplier field

Fig. 7. Comparison of rigid-block mechanism with finite element limit analysis (H/D=4, ϕ'=5°, $\gamma D/c'$=1, smooth interface).

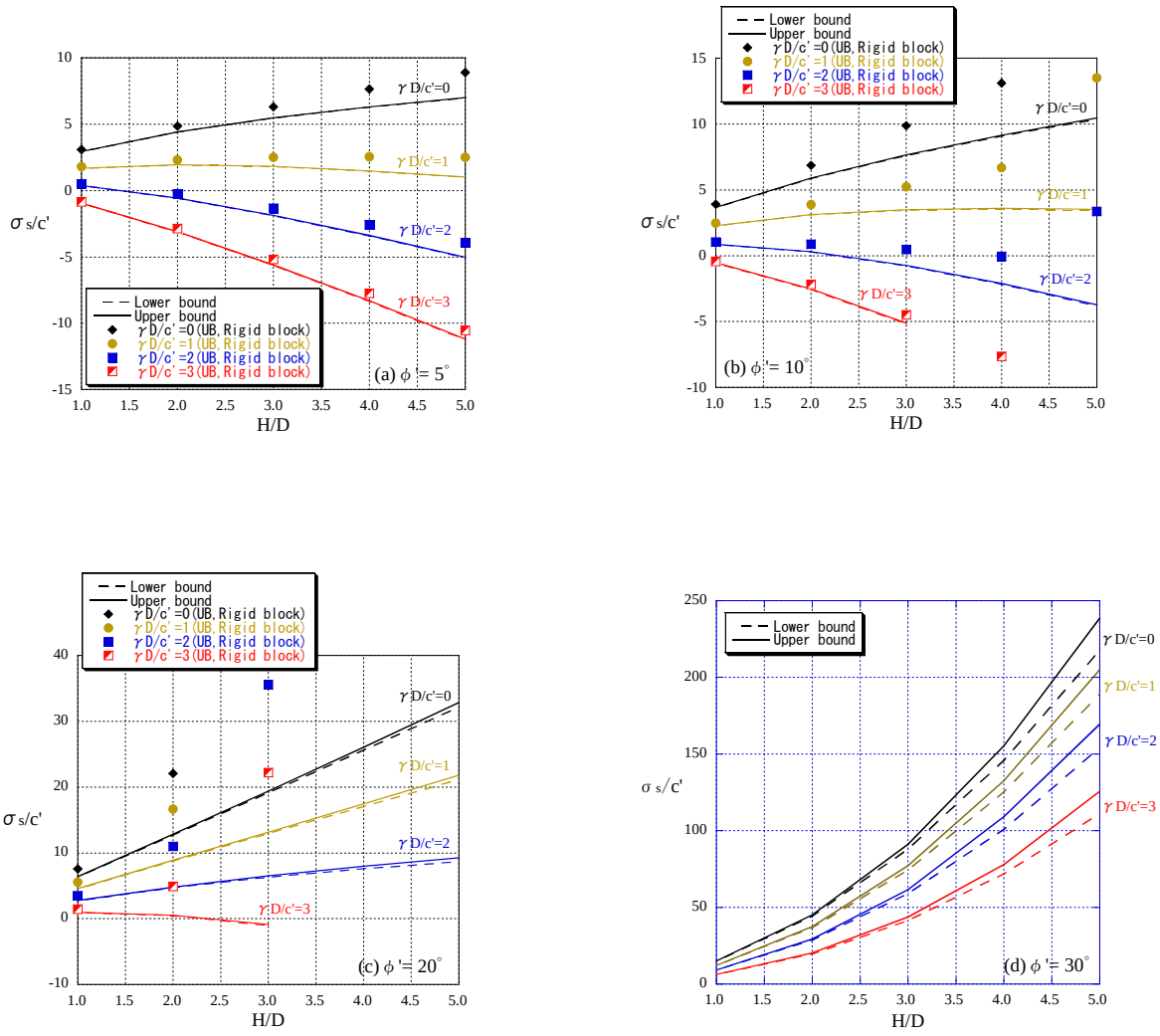

Fig. 8. Stability bounds for a circular tunnel (ϕ'=5º, 10º, 20º, and 30°, smooth interface).

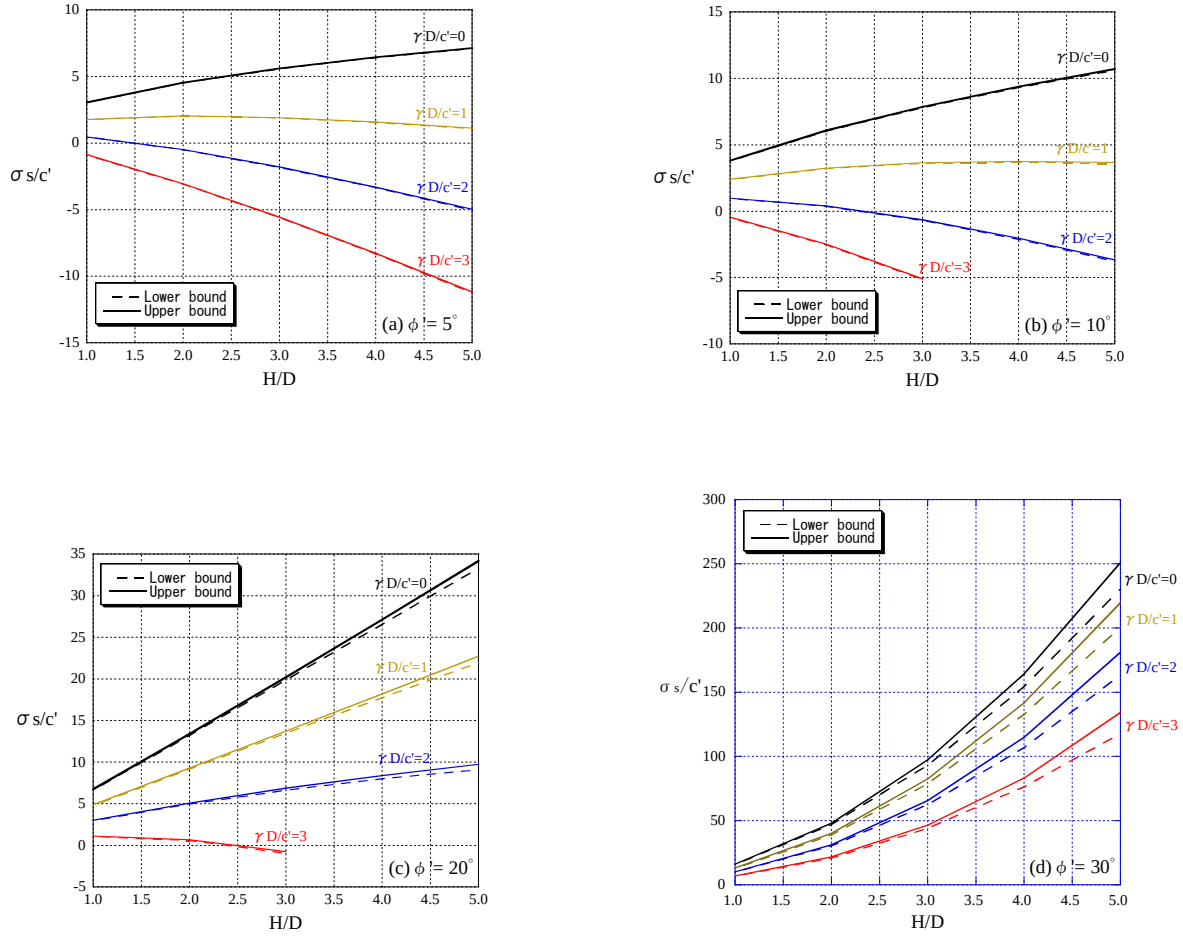

Fig. 9. Stability bounds for a circular tunnel (ϕ'=5º, 10º, 20º, and 30°, rough interface).